Proceedings 10th NUMGE 2023
10th European Conference on Numerical Methods in Geotechnical Engineering
Zdravkovic L, Kontoe S, Taborda DMG, Tsiampousi A (eds)

https://doi.org/10.53243/NUMGE2023-438

Accounting for effects of cyclic loading in design of offshore wind turbine foundations

H.P. Jostad[1], H. Liu[1], N. Sivasithamparam[1]

[1]*Norwegian Geotechnical Institute (NGI), Oslo, Norway*

ABSTRACT: In the design of foundations for offshore structures, it is generally important and required to consider the effects of cyclic loading caused by waves and wind. Therefore, NGI has developed a framework since the early 1970s that has been utilized in the design of various offshore structures. However, there are currently no accepted guidelines on how to account for this effect in design of monopile foundations. With the introduction of large-diameter monopile foundations for offshore wind turbines, it has become necessary to revisit and modify our existing procedure. The primary difference between monopile foundations for offshore wind turbines and those for the oil and gas industry is that the design of the former is typically not governed by a global failure mechanism during extreme storm loading because of their rather ductile response. Additionally, offshore wind parks often consist of over one hundred turbines, which necessitates more efficient design methods to optimise each individual foundation within a huge field with varying soil stratigraphy. This paper presents an efficient procedure using the finite element method to account for the effects of cyclic loading in design of monopile foundations. Furthermore, it provides recommendations for further improvements.

Keywords: Monopile foundations; cyclic loading; FEM; design; offshore wind turbines

1 INTRODUCTION

When designing foundations for offshore structures, it is generally important and required to consider the effects of cyclic loading caused by waves and wind (DNV, 2016). However, there are currently no official recommendations on how to account for this effect in the design of monopile foundations, except the description in DNV (2019).

With the introduction of large-diameter monopile foundations for offshore wind turbines (OWT), it has become necessary to revisit and adjust our existing procedures. The primary difference, compared to typical foundations for fixed platforms used in the oil and gas industry, is that the design of monopile foundations is usually not governed by a global failure mechanism during extreme storm loading because of their rather ductile response. Another challenge is that offshore wind parks may consist of over one hundred turbines, requiring more efficient design methods to optimise each individual foundation within a huge field with varying soil stratigraphy. As a result, the available geotechnical data at each location is also more limited than for oil and gas developments.

NGI has since 1970s developed calculation procedures that has been used in design of various offshore structures (Andersen et al., 1988, Andersen and Lauritzsen, 1988, Andersen and Høeg, 1991, Andersen and Jostad, 1999, Andresen et al., 2011, Jostad et al. 2023). This paper presents a procedure where the response of monopile and soil for different design limit states is established by efficient finite element analyses (FEA), taking into account the effects of cyclic loading. Furthermore, the paper provides recommendations for potential improvements of the proposed procedure.

2 BEHAVIOUR OF MONOPILE FOUNDATIONS

Monopile foundations are subjected to wave and rotor-influenced wind loads that are varying in time as illustrated in Figure 1.

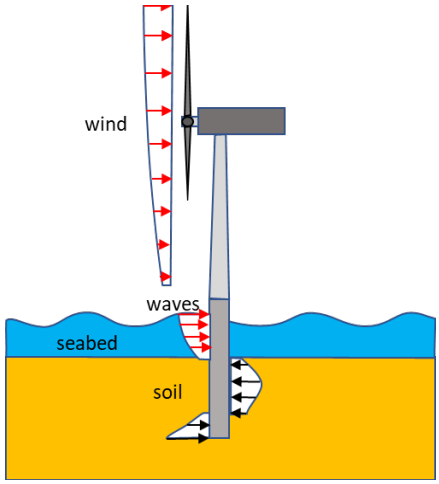

Figure 1. Loads on OWT with monopile foundation.

These loads depend on the water depth and the environmental condition at the actual location (Bachynski et al., 2019) together with the lay-out of the turbine and the geometry of the substructure.

In addition, since monopile substructures are dynamically sensitive the response also depends on the stiffness of the foundation. This stiffness is non-linear and may vary in time due to cyclic degradation of the soil (Figure 2).

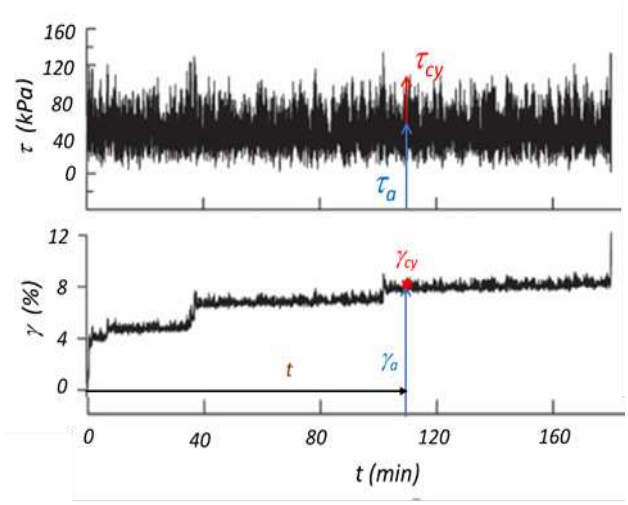

Figure 2. Time dependent average and cyclic shear stress-strain relationship (after Skau et al. 2022).

One way of accounting for this non-linear and time dependent behaviour of the foundation stiffness in time domain analyses is to describe it by a macro-model (e.g. Page et al., 2018). A macro-model is a mathematical formulation of the relationships between forces/moments and displacements/rotations at a given point, for instance at seabed. This means that the degrees of freedom of the foundation are reduced to 3 displacements and 3 rotations. The macro-model may account for:

- The non-linear behaviour of the foundation response
- The coupling between forces and moments which may act in different directions
- Different stiffnesses during loading and unloading, which also results in hysteretic damping
- Degradation of the stiffness with time due to cyclic loading
- Accumulation of displacement/rotation with time due to cyclic loading

However, the input to the macro-model needs to be established by analyses of the monopile foundation and the surrounding soil.

In Ultimate Limit State (ULS) and Serviceability Limit State (SLS), it is the displacements and rotation of the monopile at the occurrence of extreme loads and at the end of lifetime that need to be checked. In these cases, the same approach as used for other offshore structures as that described in DNV (2019) can be used.

3 CYCLIC BEHAVIOUR OF SOIL

In this section the characteristic behaviour of soil subjected to cyclic loading is briefly presented. The presented results are mainly based on information given in Andersen (2015). However, different aspect of this behaviour may be found in several other papers (Yasuhara et al., 1992; Wichtmann et al., 2010; Zografou et al., 2019, etc.).

3.1 Cyclic shear stiffness

The most important behaviour of the soil that affects the design of monopile foundations is that the stiffness is highly non-linear, starting from a maximum small-strain stiffness G_{max} at zero cyclic shear stress ($\tau_{cy} = 0$) as shown in Figure 3. The actual non-linear behaviour depends on the soil, previous load history (e.g. over-consolidation ratio OCR, cyclic loading, drainage condition, etc.), stress path and strain rate. Therefore, an appropriate description of this non-linear behaviour needs many parameters.

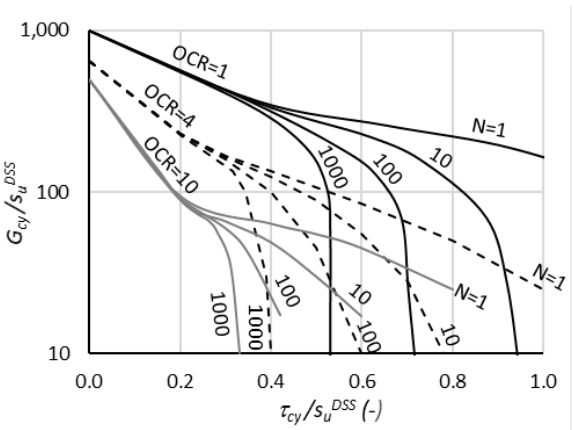

Figure 3. Secant cyclic shear modulus G_{cy} normalized by the undrained direct simple shear strength s_u^{DSS} versus normalized cyclic shear stress τ_{cy}/s_u^{DSS} after N=1, 10, 100 and 1000 cycles. Drammen clay with OCR=1, 4 and 10. Normalized average shear stress τ_a/s_u^{DSS}=0 (after Andersen, et al., 1988).

3.2 Effect of average shear stress

Different average shear stress levels will change the cyclic shear modulus as illustrated in Figure 4. The effect of the average shear stress level is generally larger for triaxial stress paths than direct simple shear paths and larger for sands than clays.

3.3 Accumulated shear strain

Another effect of the average shear stress is development of average (or accumulated) shear strain. The average shear strain γ_a, will increase with increasing number of cycles, increasing cyclic shear stress level and increasing average shear stress level. This is illustrated in Figure 5.

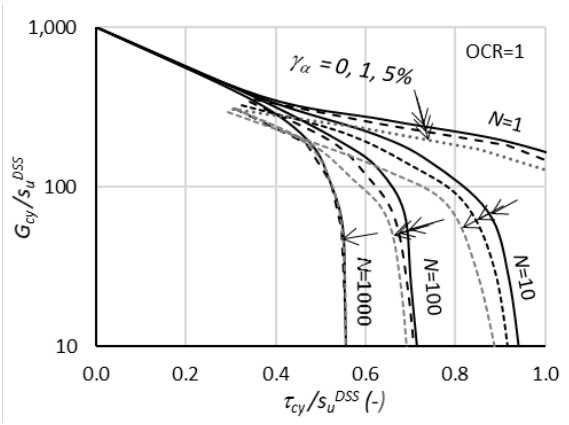

Figure 4. Normalized secant cyclic shear modulus G_{cy}/s_u^{DSS} versus normalized cyclic shear stress τ_{cy}/s_u^{DSS} after N=1, 10, 100 and 1000 cycles. Drammen clay with OCR=1 and γ_a = 0, 1 and 5% (based on data in Andersen, et al., 1988).

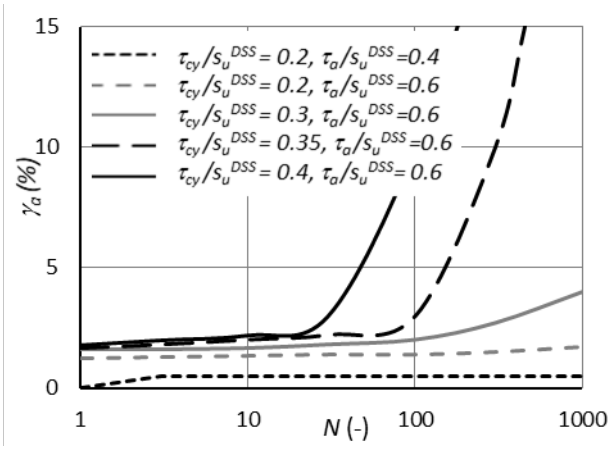

Figure 5. Development of the average shear strain γ_a versus number of cycles. Drammen clay with OCR=1, τ_{cy}/s_u^{DSS}= 0.2, 0.3, 0.34 and 0.4, and τ_a/s_u^{DSS}=0.4 and 0.6 (based on data in Andersen, et al., 1988).

3.4 Cyclic load history

In this paper, it is assumed that the soil around the monopile is undrained at least during one single load cycle. This assumption is based on coupled pore water flow and displacement (consolidation) analyses shown in Li et al. (2019), where it is shown that even sand is nearly undrained during a single cycle. This means that the cyclic stiffness of the soil can be based on results from undrained laboratory element tests starting from the actual drained stress state (σ_{vo}' and σ_{ho}'). From this state one may have different combinations of undrained average and cyclic shear stresses (τ_a and τ_{cy}) along different stress paths (e.g. triaxial compression, direct simple shear and triaxial extension) that both are continuously varying with time. An example of this stress history and the corresponding measured response are shown in Figure 2. More details about these tests may be found in Skau et al. (2022) and Liu et al. (2022).

However, this is just a stress history for one example of a 3-hours peak storm period that is very useful for verification of material models and calculation procedures. In design, one need to consider different load histories and longer periods. For this purpose, it is more convenient to base the soil behaviour on standard monotonic and cyclic laboratory element tests. Results from a large number of these types of tests are for instance presented in Andersen (2015). Together with the standard tests, one need a procedure to calculate the time dependent change in the response due to irregular cyclic loading as will be discussed in the next section.

3.5 Effect of previous cyclic stress history

As discussed in the previous sections, the behaviour or response of the soil change with time (or number of cycles) when subjected to cyclic loading. This change in behaviour can be determined from standard cyclic laboratory tests. However, since during storm loading both the average and cyclic stresses will change with time (Figure 2) one cannot use the actual number of cycles as a time dependent state parameter. NGI has therefore by considering different cyclic stress histories on different clays, studied several alternatives (Andersen et al., 1992).

For clay it was found that the present secant cyclic shear modulus G_{cy} (Figure 3) is a good measure for the behaviour of the clay since it directly accounts for the cyclic degradation of the soil. The reduction in G_{cy} captures the effect of reduced mean effective stress p' due to accumulated pore pressure, but also changes in the structure/fabric of the soil due to accumulated shear deformations γ_a (Figure 4).

However, due to the non-linear behaviour of the soil, G_{cy} depends on the applied cyclic shear stress τ_{cy}. Therefore, we use a constant cyclic shear stress τ_{cy} and the corresponding cyclic shear strain γ_{cy} after a number of cycles N (sometimes imprecisely just called equivalent number of cycles without defining at which cyclic shear stress level) as a measure for the effect of a varying average and cyclic stress history.

The use of this approach is illustrated in Figure 6 where the same cyclic shear stress is applied at the end of two different cyclic shear stress histories. The irregular history is a representative history for a soil element around a monopile in clay during extreme storm loading. The other history is an idealised representation of the same history, i.e. the same number of cyclic shear stresses grouped as packages of equal τ_{cy} in ascending order.

Figure 6 shows that the response (cyclic shear stress-strain loop) during the test cycle at the end of the two different stress histories are rather similar. It is therefore assumed that the behaviour of the soil after these two different histories is also similar. The corresponding equivalent number of cycles at this shear stress level can then be found from a test with a constant number of this

cyclic shear stress. More details about these tests can be found in Skau et al. (2022) and Liu et al. (2022).

Often, it is the combination of equivalent number of cycles to failure and the corresponding cyclic shear stress that is used in ULS design. However, in design of monopile foundations the shear stress level even close to the monopile is not necessary at failure at the maximum design load. Therfore, it is more correct to use the equivalent number of cycles at the actual cyclic shear stress level to account for the cyclic effect. This approach will be demonstrated in an example calculation in Section 4.3.

From Figure 3, it is seen that the cyclic degradation, i.e. reduction in the secant cyclic shear modulus, is small below a given cyclic shear stress level. This means that the equivalent number of cycles is undefined below this shear stress level. The same response is obtained at one cycle and after a large number of cycles. A large equivalent number of cycles below this shear stress level should therefore not be interpreted as large cyclic degradation.

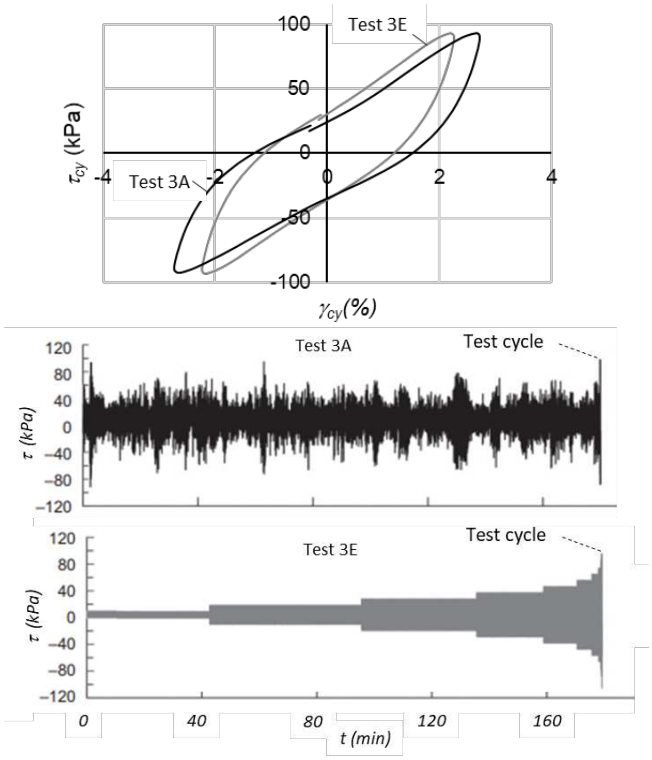

Figure 6. At top, shear stress-strain loops for a test cycle at the end of the two different load histories shown below (after Skau et al., 2022).

This concept of equivalent number of undrained cycles at a constant cyclic shear stress level that results in a given secant cyclic shear modulus is used in a procedure where an idealized shear stress composition, i.e. packages of number of cycles of different constant cyclic shear stress levels, as shown in Figure 6, is used to calculate the cyclic stiffness of soils for a design condition.

In this procedure, it is necessary to consider the non-linear behaviour of the soil, in which the secant cyclic shear modulus decreases as the cyclic shear stress level increases at a given stress state, and conversely, increases as the cyclic shear stress level decreases. One cannot just use the same curve at the same number of cycles, because it is two different tests at two different cyclic shear stress levels as shown in Figure 7. Instead, one need to construct the actual response at the same stress state and same cyclic degradation. For simplicity, this is often done by assuming that the cyclic shear strain between the two cyclic shear stress levels is the same as the change after cycle number 1 (N=1) at these two cyclic shear stress levels as shown later in Figure 13. Then one finds the curve for a given number of cycles at this shear stress level that fits this cyclic shear strain as shown in Figure 13. This is then the equivalent number of cycles at this new shear stress level that gives the same cyclic degradation of the non-linear secant cyclic shear modulus as in the last cycle of the previous cyclic shear stress level. This construction of the shear stress-strain curve is an approximation. However, the inaccuracy becomes limited if the difference in shear stress levels between two shear stress packages are small. Furthermore, it is also checked that the assumption is reasonable by studying results from tests with idealized packages as shown in Figure 6. The last cycle in one package and the first cycle in the next package is shown in Figure 7. The equivalent number of cycles that gives this cyclic shear strain or secant cyclic shear modulus can then be found by a cyclic laboratory test at this new shear stress level (or interpolated between existing tests as shown in Figure 13).

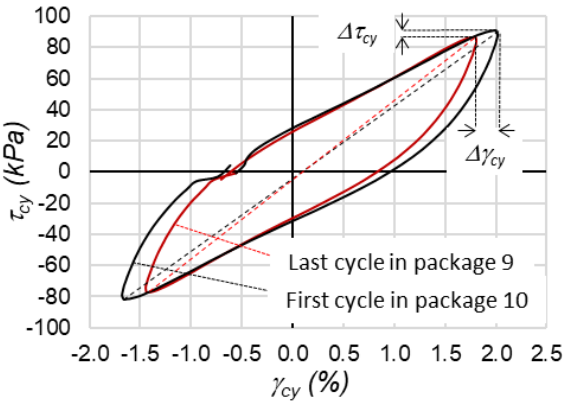

Figure 7. Change in secant cyclic shear stiffness when the cyclic shear stress is changed at a given stress state. From Test 3E with packages of different cyclic shear stresses in Figure 6.

For sand, the cyclic degradation may also be defined by the change in cyclic shear modulus. However, since the behaviour of the sand around the monopile is not undrained during several cycles, the effect of combined pore pressure accumulation and dissipation needs to be considered. For this reason, it is more convenient to determine the cyclic degradation by the equivalent number of undrained cycles required to generate an excess pore

that correspond to the time dependent change in mean effective stress $\Delta p'$ from a reference mean effective stress p_o'. In the undrained cyclic element laboratory tests, the reference mean stress p_o' is the effective mean (consolidation) stress prior to the undrained cyclic phase. In addition, when the cyclic shear stress level is changing from one cycle to the next the effective mean stress may also change. This procedure is for instance used in the Partially Drained Cyclic Accumulation Model (PDCAM) as described in detail in Jostad et al. (2015).

Knowing the equivalent number of undrained cycles N_{eqv} at different cyclic and average shear stress levels for a given soil, the corresponding cyclic and average shear strain can be interpolated from cyclic laboratory tests or contour diagrams as shown in Figure 8.

3.6 Average and cyclic shear stress-strain relationships

The number of cyclic laboratory tests at a given location and depth where a monopile foundation is planned to be installed are generally limited.

Therefor at NGI, we use the available test results together with information from a large number of existing laboratory tests to establish so-called contour diagrams as described in Anderson (2015). Figure 8 shows an example of a diagram with the relationships between normalized average and cyclic shear stress τ_a/s_u^{DSS} and τ_{cy}/s_u^{DSS}, average and cyclic shear strain γ_a and γ_{cy} versus number of cycles N from undrained cyclic and monotonic DSS tests. This type of diagram may be used to establish: a) the secant cyclic shear modulus as function of cyclic shear stress level, average shear stress level and number of cycles as shown in Figure 4; b) calculate the equivalent number of cycles for an idealised shear stress composition; c) establish the non-linear shear stress-strain curve (sum of average and cyclic components) at the occurrence of the maximum design loads as shown in Figure 2; and d) determine the accumulated shear strain as function of number of cycles as illustrated in Figure 5.

In some special cases these diagrams can even be established without any site-specific cyclic tests but instead based on correlations with index properties as Plasticity Index (clays), relative density (sands), water contents (clay/silt/sand), over-consolidation-ratio (clay/silt/ sand), etc. The accuracy in the behaviour is then questionable; however, it is still assumed to be better than not using this information.

There is therefore a need for additional laboratory test programs to better understand the background for the relationships defined by these diagrams. With enough tests, machine learning (ML) algorithms may be used to establish better relationships between index data and the shape of these contour diagrams.

The development of advanced constitutive models based on fundamental concepts as for instance the critical state concept, may also be used to improve the development and to increase the understanding of the shape of these contour diagrams. However, as for instance shown for sand, micro-mechanical effect as fabric changes during cyclic loading is not fully understood and properly accounted for in these models (Jostad et al., 2020), thus limit the accuracy of these models. Similar type of limitation is also assumed to be the case for describing the cyclic behaviour of silts and clays. More research is therefore required to better understand the micro-mechanical effects of cyclic loading and by this improve these models.

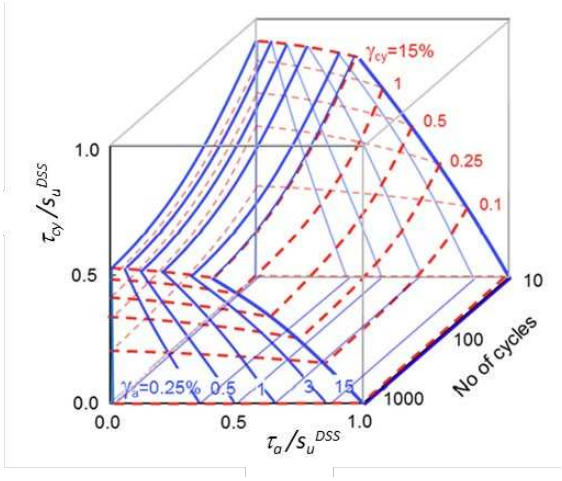

Figure 8. Example of a 3D cyclic contour diagram based on DSS tests on a normally consolidated (OCR=1) Drammen clay (after Jostad et al.,2014).

For clean sand we have obtained interesting results showing that contour diagrams could be calculated by the discrete element method LS-DEM where a representative geometry of the individual grains is described by level-set (LS) functions (Kawamoto et al., 2018). Some initial trial simulations were presented in Jostad et al. (2021).

4 FINITE ELEMENT ANALYSES

4.1 Back-ground information

The history and stress-path dependent non-linear shear stress-strain relationships in the soil around the monopile are accounted for by the Undrained Cyclic Accumulation Model (UDCAM) as described in (Jostad et al., 2014) or the Partially Drained Cyclic Accumulation Model (PDCAM) as described in (Jostad et al., 2015). In these two models the stress-strain relationships are continuously updated in each integration point depending on the actual cyclic stress path history following the procedure described in the previous section. The analyses are in the time domain following an idealized load composition with packages of different constant aver-

age loads and number of constant cyclic loads. By stepping forward in time (where each step may contain several cycles) the average and cyclic shear stresses are continuously updated. The stress path dependency follows the ADP concept, as used in NGI-ADP (Grimstad et al. 2012), by interpolating between laboratory results from Active (compression) triaxial test, Direct Simple Shear (DSS) tests and Passive (extension) triaxial tests depending on the orientation of the maximum principal stress compared to the vertical axis. This is different from accounting for the effect of the intermediate principal stress as often used in other constitutive models. Since the analysis does not follow each cycle, any inertia effects need to be accounted for in the applied loads.

These calculations may still be time-consuming, sometimes unstable and involve coupling between average and cyclic calculation phases that needs some special scripting. Therefore, a simplified procedure was proposed in (Jostad et al., 2023). A short summary of this simplified procedure is described below.

4.2 A simplified cyclic FEA approach

In this proposed simplified procedure for calculating the monopile response any suitable finite element codes and constitutive models for describing the undrained non-linear shear stress-strain relationships of the soil around the monopile may be used. The time or history dependent cyclic stress-strain curves are calculated prior to each finite element analyses. The actual cyclic shear stress history in the soil is found by an interative procedure. In each finite element analysis the monopile loads are increased monotontically to their maximum values following steps according to the actual idealized load composition (sum of average and cyclic components in each package).

Based on this, the simplified procedure consists of the following steps:

1. Establish an idealized global cyclic load composition of the monopile design loads together with a constant cyclic to average load ratio. How this can be done is for instance described in (Norén-Cosgriff et al., 2015).
2. Establish the history and stress path (ADP) dependent non-linear undrained shear stress-strain curves of each material cluster (e.g. in selected sublayers along the monopile). For instance in the first iteration, either N=1 can be assumed or N=N_{eqv} can be calculated based on the global load composition scaled to different maximum shear stress levels.
3. Calibrate the applied consitutive model to the established shear stress-strain curves for each material cluster.
4. Increase the global loads monotonically in a finite element analysis by steps according to the load composition given in Step 1.
5. Extract the calculated local cyclic soil reaction (or shear stress) composition in each material cluster.
6. Calculate $N = N_{eqv}$ for each material cluser as described in the previous section and demonstred for a clay layer in the next sub-section.
7. Continue from Step 2 until the solution has converged.

This iterative procedure generally converges after 1 to 3 iterations. For clays this iterative procedure can be preformed using the UDCAM-S model/procedure in Plaxis (Brinkgreve et al., 2023).

The above procedure, where a constant cyclic to average load ratio needs to be assumed, could be refined by dividing the analyses into average and cyclic calculation phases. Furtheremore, by defining material clusters in different zones around the monopile the simplified procedure may approach toward a full UDCAM analysis as described in (Jostad et al., 2014).

In the following section, the proposed simplified procedure is used to analyse a simplified 2D problem. The purpose of the example is to demonstrate the different tasks given above. Therefore, it is not meant to study the effect of cyclic degradation around a monopile for a real design case.

4.3 Example: Idealized 2D problem

A 2D vertical cross-section through a monopile foundation in a normaly consolidated (OCR=1) clay is considered. It is realised that this is not a realistic analysis of a monopile, it is just for simplicity used for demonstration purpose. The finite element software Plaxis 2D together with the UDCAM-S model/ procedure (Brinkgreve et al., 2023) are used.

The diameter of the monopile is 6 m and the penetration depth into the clay is 30 m. The monopile and the soil plug are considered as an equivalent solid material with a Youngs modulus of 11.2 GPa and a Poisson ratio of 0.2. The ratio between the overturning moment and the horizontal force at seabed is 27 m. The maximum horizontal load H_{max} = 780 kN/m.

The cyclic load composition consists of only two load packages of one-way cyclic loads, i.e. with a cyclic to average load ratio of 1. The first package consists of 100 cycles with a maximum load that is 80% of H_{max} (0.8 · 780 = 624 kN/m). Then the second and final package of 1 cycle of H_{max} = 780 kN/m. Figure 9 shows the finite element mesh used.

The width of the model is 160 m and the depth of the soil is 80 m. The horizontal load is applied at the top of the monopile, 27 m above seabed. The soil along the monopile is diveded into 6 horizontal sublayers each with a thickness of 5 m. A 5 m thick layer is also

included below the monopile. The model consists of 1211 15-node triangular elements. Interface elements are used between the monopile and the soil. Full roughness is for simplicity assumed for the interfaces. Altough, an interface strength that accounts for installation and time dependent set-up effects should be used in design.

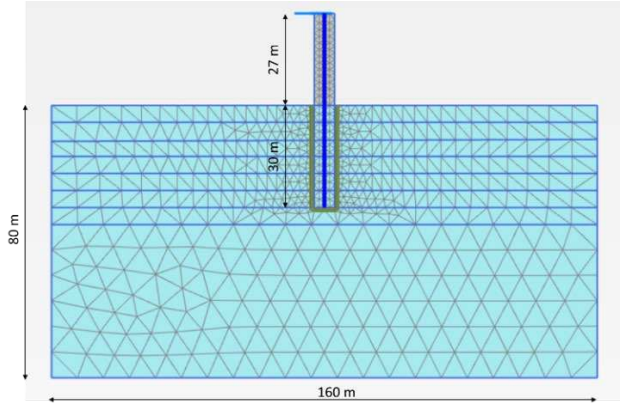

Figure 9. Finite element mesh.

The non-linear cyclic shear stress-strain behaviour of the clay are based on Drammen clay with OCR=1 (Andresen, 2015). Figure 10 shows the cross sections through the 3D contour diagrams for DSS condition at N=1 and 10. In this cross sections the shear stresses τ_a and τ_{cy} are normalized by the undrained triaxial compression strength s_u^C where the ratio $s_u^{DSS}/s_u^C = 0.64$ and s_u^{DSS} = 2.1 kPa/m · depth (m). In the analysis, it is for simplicity assumed an isotropic undrained shear strength equal to s_u^{DSS} and thus an effective horizontal to vertical initial stress ratio K_o=1.

The normalized shear stress-shear strain curves here given as the sum of the cyclic and average shear stresses and strains in the cross sections N=1 and 10 in Figure 10 are shown in Figure 11. For this cyclic to average shear stress ratio of 1, the problem is mainly govern by the development of increased average shear strains during cyclic loading. This will give some permanent tilt of the monopile at the end of the cyclic load history.

The interpolated points in Figure 11 are used to calibrate the material properties of the NGI-ADP model also available in Plaxis. A good fit to the points is obtained by G_o/s_u^{DSS} =1000 which is equal to the small strain stiffness shown in Figure 2 and a cyclic history independent failure strain (sum of cyclic and average component) of γ_f^{DSS} = 10%. To account for the effect of cyclic degradation, it is found that the fitted normalized peak undrained shear strength (sum of cyclic and average components) will reduce from $\tau_{cy,f}^C / s_u^C = 0.94$ at N=1, to 0.88 at N=3 and 0.82 at N=10. These values are then divided by the anisotropy ratio of s_u^{DSS}/s_u^C =0.64, since s_u^{DSS}/depth = 2.1 kPa/m is used as input strength with depth. An istropic shear strength is obtained by input of $s_u^{DSS}/s_u^C = s_u^E/s_u^C$ =1.

Figure 12 shows the calculated distribution of the resultant normal contact stress p from the soil (active plus passive side) versus depth after iteration zero (N=1) for 80% and 100% of H_{max}. These stresses are used to calculate local cyclic load compositions and a representative cyclic shear stress levels at the maximum load for each sub-layer as given in Table 1.

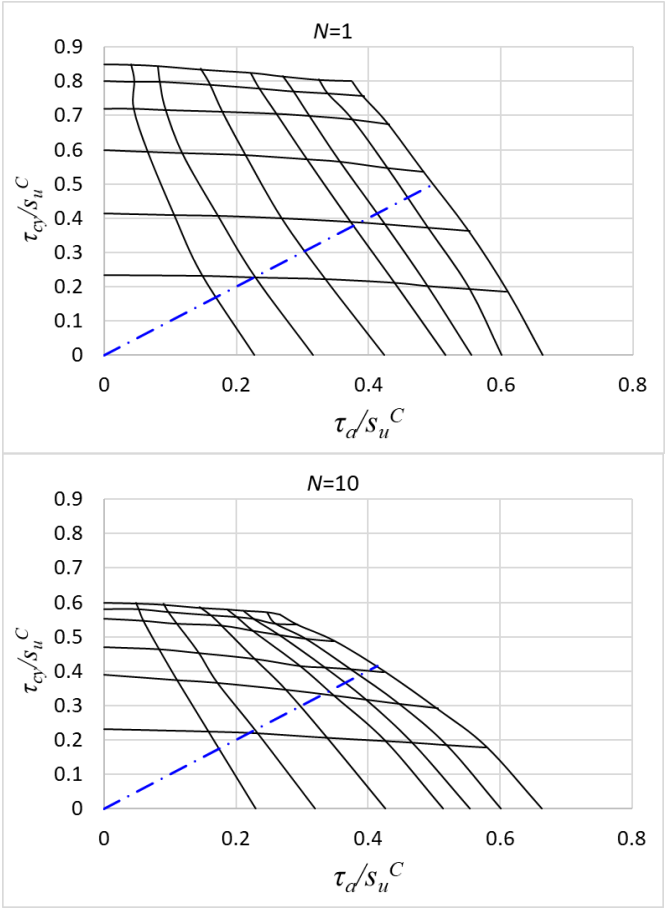

Figure 10. Cross section at N=1 and 10 through the 3D contour diagram for DSS condition. Drammen clay with OCR=1. Shear stresses normalized by s_u^C/s_u^{DSS} =1.56.

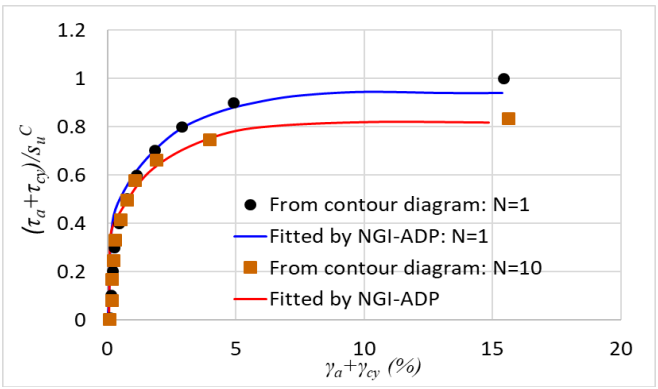

Figure 11. Normalized *shear stress-strain curve for N=1 and 10, τ_{cy}/τ_a = 1, fitted with the NGI-ADP model.*

The cyclic component of the normal stress p_{cy} is 50% of p (cyclic to average load ratio of 1). The local cyclic load ratio between Parcel 1 and Parcel 2 is p_{cy} at 80% divided by p_{cy} at 100% of the maximum load (p_{80}/p_{100}).

Table 1. Soil pressures p and N_{eqv}. Iteration=0

Sub-layer	z (m)	p_{80} (kPa)	p_{100} (kPa)	p_{80}/p_{100}	p_f (kPa)	p_{cy}/p_f	N_{eqv}
1	2.5	31	38	0.81	27	0.71	8
2	7.5	80	100	0.80	81	0.62	10
3	12.5	109	140	0.78	135	0.52	20
4	17.5	110	147	0.75	189	0.39	6
5	22.5	62	84	0.73	243	0.17	1
6	27.5	-121	-163	0.74	297	0.27	1

Table 2. Soil pressures p and N_{eqv}. Iteration=1

Sub-layer	z (m)	p_{80} (kPa)	p_{100} (kPa)	p_{80}/p_{100}	p_f (kPa)	p_{cy}/p_f	N_{eqv}
1	2.5	33	35	0.93	27	0.65	6
2	7.5	81	97	0.84	81	0.60	17
3	12.5	110	144	0.77	135	0.53	11
4	17.5	114	157	0.73	189	0.42	5
5	22.5	65	91	0.71	243	0.19	1
6	27.5	-126	-178	0.71	297	0.30	1

The corresponding monotonic stress at failure $p_f = N_c \cdot s_u^{DSS} = 5.14 \cdot 2.1 \cdot z$ is used to normalize the cyclic pressure p_{cy}. This gives a representative cyclic shear stress mobilisation of p_{cy}/p_f. In the cyclic strain accumulation carried out here it is assumed that the cyclic shear stress level τ_{cy}/s_u^{DSS} in each sub-layer at H_{max} is equal to p_{cy}/p_f. The above values for the first iteration are presented in Table 1. Based on these values the equivalent number of cycles N_{eqv} at the cyclic shear stress level during the last load parcel is calculated using the procedure described in Section 4.2. Figure 13 shows the calculation for Sub-layer 1 in Iteration=0.

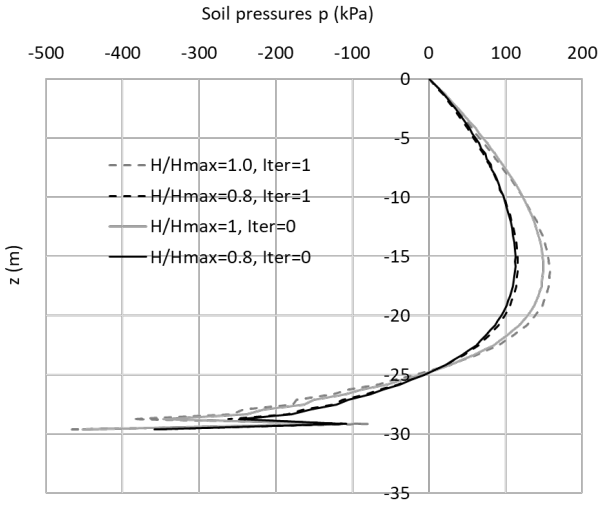

Figure 12. Calculated resultant normal soil stress p against the monopile versus depth z after iteration 0 (N=1) and iteration 1 (N=N_{eqv}).

At the beginning of Parcel 2 with $\tau_{cy}/s_u^{DSS} = p_{cy}/p_f$ =0.71, N_{eqv} = 7 is determined, as shown in Figure 13. The same calculation is done for the other sublayers and N_{eqv} at Parcel 2 is given in Table 1. At low cyclic shear stress levels the cyclic degradation is negligible (Figure 3) and N=1. The corresponding cyclic plus average shear stress-strain curves are fitted by the NGI-ADP model with varying $\tau_{cy,f}^C/s_u^C$ versus N_{eqv} as described above. These stress-strain curves are then used in an updated finite element analysis (Iteration 1). The new calculated resultant normal stress p against the monopile is also included in Figure 12. It is seen that the stresses are slightly reduced in the upper two sublayers (1 and 2), increased in Sublayers 3, 4 and 5, and more or less unchanged in Sublayer 5 (below the centre of rotation).

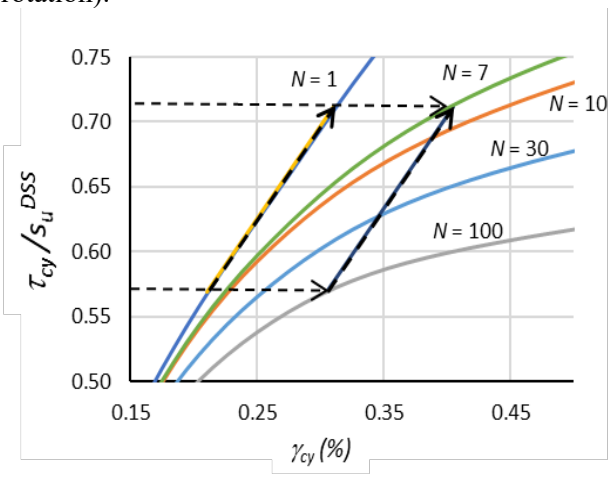

Figure 13. Calculation of N_{eqv}=7 at the beginning of Parcel 2 for sub-layer 1 based on results from Iteration 0.

Based on these updated stress distrubutions, the values in Table 2 are calculated in the same way as for Iteration 0. However, these changes in N_{eqv} gave small changes in the calculated response, and the solution has therefore converged.

Figure 14 shows the calculated horizontal displacement at seabed u_x of the monopile in Iteration 0 and Iteration 1 when the maximum horizontal load H_{max} is increaded from 0 to 1 in Parcel 2. The maximum displacement at seabed has increased from 0.39 m to 0.52 m due to degradation in the cyclic stiffness and accumulation of average shear strains during the 100 cycles in Parcel 1.

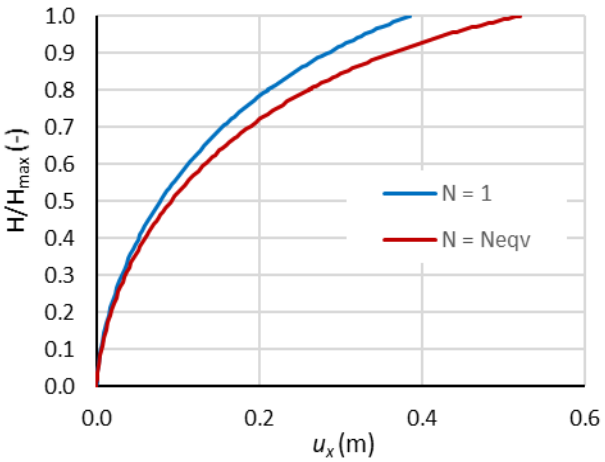

Figure 14. Calculated horizontal displacement of the monopile u_x at seabed versus normalized load H/H_{max} after iteration 0 (N=1) and iteration 1 (N=N_{eqv}).

For ULS condition, it is only the calculated displacement and rotation at the maximum environmental loads during a design storm that are of interest. These values should be less than some project dependent allowable values. The calculated non-linear curve is thus not used in the design process.

A similar approach may be used to calculate the cyclic displacements and rotations or cyclic foundation stiffnesses. Only the cyclic components of the shear stress-strain relationships are then used in the finite element analyses. Cyclic stiffnesses are needed to calculate the dynamic response of OWT.

These calculations can be easely carried out in 3D FEA as shown in (Jostad et al., 2023) and therefore used in design of monopile foundations. At NGI, we are using a very efficient finite element program called INFIDEP (Sivasithamparam and Jostad, 2021) in these types of analyses.

5 CONCLUSIONS

The paper presents the characteristic behaviour of soil subjected to cyclic loading and how this may be taken into account in history or time dependent non-linear shear stress-strain relationships. These stress-strain curves may be fitted by a suitable consitutive model and used to calculate the non-linear load-displacement relationships for OWT substructure foundations. These results may further be used as: (1) input to a macro-model of the foundation in time domain analyses of the OWT and the substructure; (2) to check the capacity or displacements under design loads; and (3) to calibrate non-linear soils springs along the monopile for structural design of the monopile.

How to use this approach in analyses of monopile foundations is described and demonstrated by an idealized example.

Furthermore, the need for numerical methods to interpolate between a limited number of soil layer dependent cyclic data was emphasised. For instance, the use of LS-DEM to simulate additional cyclic tests on clean sand looks promising and will be studied in more detail.

6 ACKNOWLEDGEMENTS

This work has been funded by the Research Council of Norway, through SFI BLUES, grant number 309281.

7 REFERENCES

Andersen, K.H., Kleven, A., Heien, D. 1988. Cyclic soil data for design of gravity structures. *ASCE, J. of Geotech. Engrg*, 114 (5), 517–539.

Andersen, K.H., Lauritzsen, R. 1988. Bearing capacity for foundations with cyclic loads. *ASCE, J. of Geotech. Engrg*, 114 (5), 540–555

Andersen, K.H., Høeg, K. 1991. Deformations of soils and displacements of structures subjected to combined static and cyclic loads. *Proceedings, X-ECSMFE*, 1147–1158.

Andersen K.H., Dyvik, R., Kikuchi, Y., Skomedal, E. 1992. Clay behaviour under irregular cyclic loading. *Proceedings. Int. Conf. on Behav. of Offsh. Structures*, 937–950.

Andersen, K.H., Jostad, H.P. 1999. Foundation design of skirted foundations and anchors in clay. *In Offshore technology conference*. OnePetro.

Andersen, K.H. 2015. Cyclic soil parameters for offshore foundation design. *Frontiers in offshore geotechnics* III (ed. V. Meyer), pp. 5–84.: CRC Press/Balkema.

Andresen, L., Jostad, H.P., Andersen, K.H. 2011. Finite element analyses applied in design of foundations and anchors for offshore structures. *International Journal of Geomechanics*, 11(6), 417-430.

Bachynski, E.E., Page, A., Katsikogiannis, G. 2019. Dynamic response of a large-diameter monopile considering 35-hours Storm Conditions. Proceedings of the ASME 2019 38th *International Conference on Ocean, Offshore and Arctic Engineering*. OMAE2019. Paper No. OMAE2019-95170

Brinkgreve, R. B. J., Kumarswamy, S., Swolfs, W.M., Waterman, D., Chesaru, A., Bonnier, P.G. 2023. PLAXIS 2023. PLAXIS bv, the Netherlands.

DNV. 2016. DNVGL-ST-0126 – Support structure for wind turbines. Oslo, Norway: DNV

DNV. 2019. DNVGL-RP-C212 Offshore soil mechanics and geotechnical engineering. Recommended Practice, DNV GL AS: Oslo, Norway.

Grimstad, G., Andresen, L., Jostad, H.P. 2012. NGI-ADP: Anisotropic shear strength model for clay. *International journal for numerical and analytical methods in geomechanics*, 36(4), 483-497.

Jostad, H.P., Grimstad, G., Andersen, K.H., Saue, M., Shin, Y., You, D. 2014. A FE procedure for foundation design of offshore structures - applied to study a potential OWT monopile foundation in the Korean western sea. *Geotechnical Engineering Journal of the SEAGS & AGSSEA*, 45(4), 63-72.

Jostad, H., Grimstad, G., Andersen, K., Sivasithamparam, N. 2015. A FE procedure for calculation of cyclic behaviour of offshore foundations under partly drained conditions. *Frontiers in offshore geotechnics III* (ed. V. Meyer), vol. 1, pp. 153–172. CRC Press/Balkema.

Jostad, H.P., Dahl, B.M., Page, A., Sivasithamparam, N., Sturm, H. 2020. Evaluation of soil models for improved design of offshore wind turbine foundations in dense sand. *Géotechnique*, 70(8), 682-699.

Jostad, H.P., Khoa, H.D.V., Karapiperis, K., Andrade, J. 2021. Can LS-DEM be Used to Simulate Cyclic Behavior of Sand? In Challenges and Innovations in Geomechanics: *Proceedings of the 16th International Conference of IACMAG*. Volume 1, 16 pp. 228-235. Springer International Publishing.

Jostad, H.P., Liu, H.Y., Sivasithamparam, N., Ragni, R. 2023. Cyclic Capacity of Monopiles in Sand under Partially Drained Conditions: A Numerical Approach. *Journal of Geotechnical and Geoenvironmental Engineering*, 149(2), 04022129.

Kawamoto, R., Andò, E., Viggiani, G., Andrade, J.E., 2018. All you need is shape: Predicting shear banding in sand with LS-DEM. Journal of the Mechanics and Physics of Solids, 111, pp.375-392.

Li, S., Zhang, Y., Jostad, H.P. 2019. Drainage conditions around monopiles in sand. *Applied Ocean Research*, 86, 111-116.

Liu, H.Y., Sivasithamparam, N., Suzuki, Y., Jostad, H.P. 2022. Load history idealisation effects for design of monopiles in clay. *Géotechnique*, 1-11.

Norén-Cosgriff, K., Jostad, H. P., & Madshus, C. 2015. Idealized load composition for determination of cyclic undrained degradation of soils. In Frontiers in Offshore Geotechnics III: Proceedings of the 3rd *International Symposium on Frontiers in Offshore Geotechnics* (ISFOG 2015) (Vol. 1, pp. 1097-1102). Taylor & Francis Books Ltd.

Page, A.M., Grimstad, G., Eiksund, G.R., Jostad, H.P. 2018. A macro-element pile foundation model for integrated analyses of monopile-based offshore wind turbines. *Ocean Engineering*, 167, 23-35.

Sivasithamparam, N., Jostad, H.P. 2021. An Efficient FEA Tool for Offshore Wind Turbine Foundations. Z. Westgate (Ed.), *4th International Symposium on Frontiers in Offshore Geotechnics*.

Skau, K.S., Dahl, B.M., Jostad, H.P., Suzuki, Y., De Sordi, J., Havmøller, O. 2022. Response of lightly over-consolidated clay under irregular cyclic loading and comparison with predictions from the strain accumulation procedure. *Géotechnique*, 1-13.

Wichtmann, T., Niemunis, A. and Triantafyllidis, T., 2010. Strain accumulation in sand due to drained cyclic loading: on the effect of monotonic and cyclic preloading (Miner's rule). *Soil Dynamics and Earthquake Engineering*, 30(8), pp.736-745.

Yasuhara, K., Hirao, K., Hyde, A.F., 1992. Effects of cyclic loading on undrained strength and compressibility of clay. *Soils and Foundations*, 32(1), pp.100-116.

Zografou, D., Gourvenec, S. and O'Loughlin, C.D., 2019. Response of normally consolidated kaolin clay under irregular cyclic loading and comparison with predictions from the accumulation procedure. *Géotechnique*, 69(2), pp.106-121.